Check for updates

Nanolayer-like-shaped MgFe₂O₄ synthesised via a simple hydrothermal method and its catalytic effect on the hydrogen storage properties of MgH₂

N. A. Ali,[a] Nurul Hayati Idris,[a] M. F. Md Din,[b] N. S. Mustafa,[a] N. A. Sazelee,[a] F. A. Halim Yap,[a] N. N. Sulaiman,[a] M. S. Yahya[a] and M. Ismail (ORCID) *[a]

In this study, the effect of nanolayer-like-shaped MgFe₂O₄ that is synthesised via a simple hydrothermal method on the performance of MgH₂ for hydrogen storage is studied. MgH₂ + 10 wt% MgFe₂O₄ is prepared by using the ball milling method. The MgFe₂O₄-doped MgH₂ sample started to release H₂ at approximately 250 °C, 90 °C and 170 °C lower than the milled and pure MgH₂ respectively. At 320 °C, the isothermal desorption kinetic study has shown that the doped sample has desorbed approximately 4.8 wt% H₂ in 10 min while the milled MgH₂ desorbed less than 1.0 wt% H₂. For isothermal absorption kinetics, the doped sample can absorb approximately 5.5 wt% H₂ in 10 min at 200 °C. Meanwhile, the undoped sample absorbs only 4.0 wt% H₂ in the same condition. The activation energy of 10 wt% MgFe₂O₄-doped MgH₂ composite is 99.9 kJ mol⁻¹, which shows a reduction of 33.1 kJ mol⁻¹ compared to the milled MgH₂ (133.0 kJ mol⁻¹). X-ray diffraction spectra display the formation of new species which are Fe and MgO after dehydrogenation, and these new species are believed to act as the real catalyst that plays a crucial role in improving the sorption performance of the MgFe₂O₄-doped MgH₂ system by providing a synergetic catalytic effect.

1. Introduction

To prepare for the future and ensure global environmental viability, energy systems have to be reliable, clean, low cost, environmentally friendly and flexible. Humanity is expected to use 40 TW of power (40 billion of kW) in the future. To satisfy this demand, different sources of renewable energy, such as hydrogen, are needed. Sustainable hydrogen is an ideal clean energy carrier because there is no carbon dioxide or other greenhouse gas emission at the end-user level. Commonly, there are 3 forms of storing hydrogen which is high-pressure gas, cryogenic liquid hydrogen in tanks (stored at 21.2 K) and as solid state hydrogen storage by either reacting with chemical compounds or absorbing. Among these approaches, solid-state hydrogen storage has higher potential for higher hydrogen density and may yield greater utility towards the practical implementation of hydrogen storage. Among the various materials for solid-state hydrogen storage, MgH₂ considered as one of the most potential material due to its high hydrogen storage capacity (7.6 wt%), excellent reversibility and low cost.[1] However, MgH₂ is restricted by the decomposition temperature,

which is high with slow sorption kinetics and is excessively stable thermodynamically.[2] Many research have been conducted to overcome these disadvantages by altering the thermodynamics and improve the kinetic properties by producing nanostructures[3,4] and utilizing catalysts such as carbon-based materials,[5,6] metals,[7–10] metal hydrides,[11,12] metal oxides,[13–18] metal halides,[19–21] and nanosized alloys.[22–24]

Previous research has proved that catalyst based on ternary metal oxides greatly improved the hydrogen storage performance of MgH₂.[15,25–35] Zhang et al.[25] demonstrate that ferrite nanoparticles (MnFe₂O₄, ZnFe₂O₄, Mn₀.₅Zn₀.₅Fe₂O₄ and CoFe₂O₄) can greatly lower the decomposition temperature of MgH₂. CoFe₂O₄ provides the best catalytic effect compared with other ferrites. New by-products are found after the dehydrogenation process, and its phase shows a great catalytic effect on the properties of hydrogen storage of MgH₂. Furthermore, Li et al.[26] shows a significant improvement in the desorption performance of MgH₂ when catalysed with MnFe₂O₄. X-ray photoelectron spectroscopy and X-ray diffraction (XRD) tests show that Fe₀.₈₇₂O and Mg₂MnO₄ phases take part as significant role in enhancing the dehydriding performance of MgH₂. Meanwhile, we showed in our previous study that MnFe₂O₄ synthesised via a simple hydrothermal method provides a remarkable effect in improving the hydrogen storage performance of MgH₂.[27] Interestingly, our result showed that Fe metal formed after dehydrogenation instead of Fe₀.₈₇₂O species, as claimed by Li et al.[26] This variation paved the way for the debate

[a]School of Ocean Engineering, Universiti Malaysia Terengganu, 21030 Kuala Terengganu, Malaysia. E-mail: mohammadismail@umt.edu.my; Fax: +609-6683991; Tel: +609-6683487

[b]Department of Electrical and Electronic Engineering, Faculty of Engineering, National Defence University of Malaysia, Kem Sungai Besi, Kuala Lumpur, Malaysia

on how ternary metal oxides, particularly ferrites, work as catalysts in improving the hydrogen sorption performance of MgH_2. Moreover, the difference in the synthesis method of the catalysts may also provide a different effect in the catalytic role.

Inspired by the role of active species that formed during the heating process in the MgH_2-ternary metal oxides catalyst system, it is quite interesting to investigate the use of other ferrites (e.g. $MgFe_2O_4$) as catalysts to improve the hydrogen sorption performance of MgH_2. Therefore, in this work, $MgFe_2O_4$ was synthesised by using a simple hydrothermal method, and its catalytic effects on the hydrogen sorption performance of MgH_2 were systematically studied. To the best of authors' knowledge, this paper is the first to study the hydrogen sorption performance of MgH_2 catalysed with $MgFe_2O_4$. The possible catalysis mechanisms of $MgFe_2O_4$ in the sorption performances of MgH_2 are also discussed in this paper.

2. Experimental details

The nanolayer-like-shaped $MgFe_2O_4$ was synthesised via a hydrothermal method. In a typical synthesis, a stoichiometric amount of $Mg(NO_3)_2 \cdot 6H_2O$ (Sigma-Aldrich) and $Fe(NO_3)_3 \cdot 9H_2O$ (Sigma-Aldrich) were dissolved in 50 ml distilled water. A total of 10 ml of $H_4N_2 \cdot H_2O$ (Sigma-Aldrich) was added dropwise to the above solution to attain the resultant pH of >9. The mixture

was then transferred into a sealed Teflon lined stainless-steel autoclave (125 ml capacity) and heated for 12 h at 180 °C. The final product was washed several times with deionised water and dried overnight at 60 °C under vacuum. A total of 10 wt% of as-prepared $MgFe_2O_4$ was mixed with 300 mg of MgH_2 (95% pure; Sigma-Aldrich) and undergo intensive ball milling for 1 h in a planetary ball mill at the rate of 400 rpm. For comparison, pure MgH_2, and MgH_2 added with 10 wt% Fe (Alfa Aesar) and 10 wt% MgO (R&M Chemicals), respectively were also prepared under the same conditions. All preparations, including loading and weighing, were conducted in an argon atmosphere glove box (MBraun Unilab).

The onset decomposition temperature and sorption kinetic measurement for doped and undoped samples were characterised by using Sievert-type pressure–composition–temperature apparatus (Advanced Materials Corporation). For onset decomposition temperature measurement, the samples were heated from room temperature to 450 °C at a heating rate of 5 °C min^{-1} in vacuum chamber. Meanwhile, the sorption kinetics was conducted under 1.0 atm at 320 °C for desorption kinetic measurement and under 33.0 atm at 200 °C for absorption kinetic measurement. The thermal properties of the doped and undoped samples were performed using differential scanning calorimeter (DSC)/thermogravimetric analysis from Metler Toledo. With a flow of 50 ml min^{-1} argon, the samples
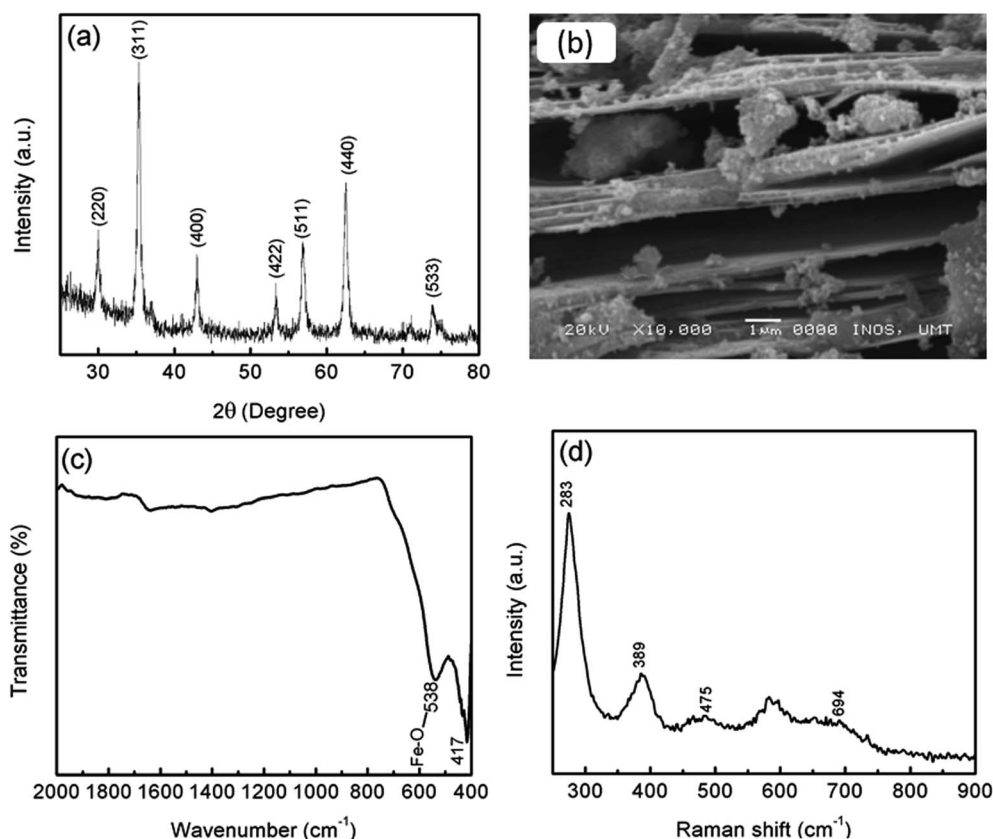

Fig. 1 (a) XRD pattern, (b) SEM image, (c) FTIR spectra and (d) Raman spectra of $MgFe_2O_4$.

were heated with 15, 20, 25 and 30 °C min^{-1} heating rate from 25 °C to 500 °C.

The phase composition of the samples was analysed by XRD *via* a Rigaku MiniFlex X-ray diffraction apparatus equipped with Cu Kα radiation. Data were collected in the 2θ range 20° to 80° at 2° min^{-1}. The morphologies of the samples were observed by scanning electron microscopy (SEM) (JEOL JSM-6350LA). Fourier transform infrared (FTIR) spectrometry was recorded on an IR Shimadzu Tracer-100 between 400 and 2000 cm^{-1}. Raman spectra were recorded on Renishaw Raman spectroscopy (532 nm radiation) extended with 0.1% power laser measurement at room temperature.

3. Results and discussion

Before milling with MgH_2, the phase structure of $MgFe_2O_4$ was confirmed by XRD, as shown in Fig. 1(a). The crystallographic planes of (220), (311), (400), (422), (511), (440) and (533) correspond to the diffraction peaks at 2θ of 30.1°, 35.4°, 43.1°, 53.5°, 57.0°, 62.6° and 74.1°, respectively. This result is in good agreement with the standard cubic spinel structure (JCPDS 71-1232). No other peaks were detected in the sample. The average crystallite size of $MgFe_2O_4$ was approximately 19 nm, as determined by using Scherrer's formula:

$$L = k\lambda/B \cos\theta, \quad (1)$$

where L is the average crystallite size (nm), θ is the angle of diffraction, k is Scherrer's constant ($k = 0.94$), λ is the X-ray wavelength (0.15405 nm) and B is the full width at half maximum of the diffraction peak in radian (FWHM). The SEM image (Fig. 1(b)) reveals that the $MgFe_2O_4$ forms a large layer with a nanosized thickness. From the FTIR spectrum (Fig. 1(c)), two typical peaks of $MgFe_2O_4$ were observed at the low wavenumber, thus indicating the formation of spinel ferrite structure.[36,37] The peak at 417 cm^{-1} can be ascribed to the Fe–O vibration in the octahedral site, and the peak at 538 cm^{-1} can be assigned to the Fe–O vibration in the tetrahedral and octahedral sites. Furthermore, the Raman peaks (Fig. 1(d)) at 475 and 694 cm^{-1} can be assigned to the typical characteristic peaks of $MgFe_2O_4$,[38] whereas the peak at 283 cm^{-1} corresponding to the stretching vibration of the Mg–O chemical bond.[39] The XRD, FTIR and Raman spectroscopy results confirm that pure $MgFe_2O_4$ was successfully synthesised by the hydrothermal method.

Fig. 2(a) shows the onset decomposition temperature results for the pure MgH_2, milled MgH_2 and MgH_2 with 10 wt% $MgFe_2O_4$. Before milling, pure MgH_2 started to desorb hydrogen at approximately 420 °C. The total amount of hydrogen desorbed is approximately 7.0 wt%. After milling for 1 h, the onset decomposition temperature of MgH_2 was decreased to approximately 340 °C. This phenomenon demonstrate that the sorption performance of MgH_2 also influenced by the milling
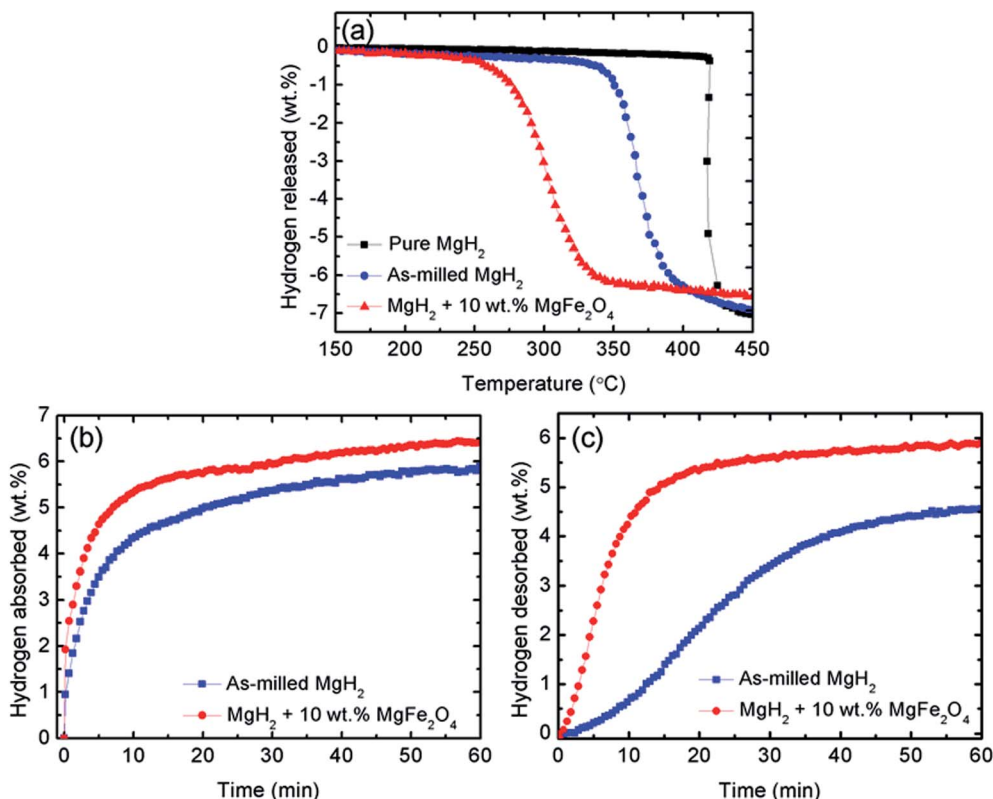

Fig. 2 (a) Decomposition temperature profile of pure and milled MgH_2, and 10 wt% $MgFe_2O_4$-doped MgH_2 sample, (b) measurement of isothermal absorption kinetics for the milled MgH_2 and 10 wt% $MgFe_2O_4$-doped MgH_2 sample at 200 °C under 33.0 atm H_2 pressures, and (c) measurement of isothermal desorption kinetics for the milled MgH_2 and 10 wt% $MgFe_2O_4$-doped MgH_2 sample at 320 °C under 1.0 atm.
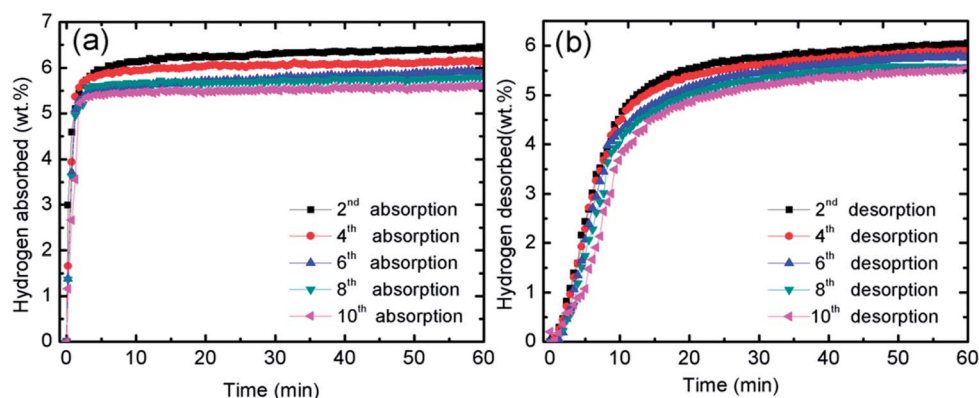
Fig. 3 (a) Measurement of isothermal absorption kinetics for the 10 wt% $MgFe_2O_4$-doped MgH_2 sample in the 2nd, 4th, 6th, 8th and 10th cycle at 320 °C under 33.0 atm H_2 pressures and (b) measurement of isothermal desorption kinetics for the 10 wt% $MgFe_2O_4$-doped MgH_2 sample in the 2nd, 4th, 6th, 8th and 10th cycle at 320 °C under 1.0 atm.

process. From the curve, it can be seen that after milling, the amount of hydrogen desorb of MgH_2 slightly decreases. This might be ascribed to the hydrogen released from MgH_2 during the milling process. After doping with 10 wt% of $MgFe_2O_4$, it is clear that the onset decomposition temperature of the MgH_2 was dramatically reduced to 250 °C, 90 °C and 170 °C lower than that for the milled and pure MgH_2, respectively. However, the hydrogen desorption capacity decrease slightly to approximately 6.5 wt% because the dopant used in this study, namely, $MgFe_2O_4$, does not contain hydrogen.[40] From Fig. 2(a), it can be concluded that $MgFe_2O_4$ additive plays a positive role in decreasing the decomposition temperature of MgH_2.

To further examine the sorption properties of the $MgFe_2O_4$-doped MgH_2 sample, the isothermal absorption kinetic was studied. The amount of hydrogen absorbed from the milled MgH_2 and the $MgFe_2O_4$-doped MgH_2 sample was measured under 33.0 atm H_2 and at constant temperature of 200 °C, as shown in Fig. 2(b). The $MgFe_2O_4$-doped MgH_2 sample shows better absorption kinetics than undoped MgH_2. For the $MgFe_2O_4$-doped MgH_2 sample, the amount of 5.5 wt% H_2 was absorbed in 10 min, whereas the milled MgH_2 only absorbed approximately 4.0 wt% H_2 within the same time. From the result, it clearly shows that the addition of $MgFe_2O_4$ enhanced the rehydrogenation kinetics of MgH_2.

For further studies on the catalytic effect of $MgFe_2O_4$ on the sorption kinetic of MgH_2, isothermal desorption kinetic was performed under 1.0 atm at 320 °C. As shown in Fig. 2(c), the $MgFe_2O_4$-doped MgH_2 sample shows significant enhancement compared with the milled MgH_2. The results shows that the undoped MgH_2 released less than 1.0 wt% H_2 after 10 min, whereas the doped sample can released approximately 4.8 wt% H_2 under the same condition. In contrast, it can be seen that $MgFe_2O_4$ also plays a significant role in enhancing the dehydrogenation kinetic of MgH_2.

The catalytic effect of $MgFe_2O_4$ was further studied with the cycling performances of $MgFe_2O_4$-doped MgH_2 system. Fig. 3(a) presents the isothermal absorption kinetics of the 10 wt% $MgFe_2O_4$ doped with MgH_2 at 320 °C under a hydrogen pressure of 33.0 atm over 10 cycles. From the result, it can be seen that

after the ten cycles, the absorption kinetics show a small reduction in the hydrogen capacity. After completing the 10th cycle, the system is able to absorb 5.6 wt% of hydrogen in 60 minutes. The result shows that the doped system displays good absorption properties even after 10 cycles. As for the desorption kinetics, Fig. 3(b) shows the isothermal desorption kinetics for 10 cycles that was carried out at 320 °C and under 1.0 atm of pressure. Like the absorption kinetics, a small hydrogen capacity degradation is shown after completing the 10th cycle. The doped system possesses a good performance after completing the 10th cycle as it is able to desorb about 5.5 wt% of hydrogen within 60 minutes. These results demonstrated that $MgFe_2O_4$ plays a vital catalytic role for the cycle life of MgH_2.

The thermal properties of the 10 wt% $MgFe_2O_4$-doped MgH_2 and undoped MgH_2 sample were further studied by DSC at heating rate of 30 °C min^{-1} and under a flow of 50 ml min^{-1} argon (Fig. 4). Obviously, the DSC trace for the pure MgH_2 showed one endothermic peak at approximately 482.9 °C. This strong endothermic peak related to the released of hydrogen
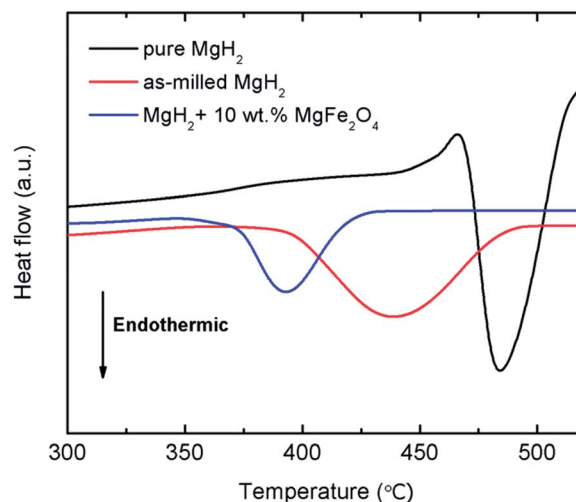

Fig. 4 DSC curves of pure MgH_2, milled MgH_2, and 10 wt% $MgFe_2O_4$-doped MgH_2.

from the MgH_2. Similar to the pure MgH_2, DSC traces of the milled MgH_2 and $MgFe_2O_4$-doped MgH_2 showed only one strong endothermic peak at 438.8 °C and 393.3 °C respectively. The peaks correlated to the decomposition of MgH_2 but at lower temperatures.

The improvement in desorption behaviour is correlated with the kinetic barrier of the hydrogen desorbed from the MgH_2. By doping MgH_2 with $MgFe_2O_4$, low value of activation energy for released hydrogen is obtained. Kissinger analysis[41] (eqn (2)) was conducted to determine the activation energy of doped and undoped MgH_2 samples.

$$\ln[\beta/T_p^2] = -E_A/RT_p + A, \tag{2}$$

where β is the heating rate, E_A is the activation energy, R is the gas constant, T_p is the peak temperature of DSC curves and A is the linear constant. Fig. 5 illustrates the curves of DSC for the milled MgH_2 and MgH_2 doping with 10 wt% $MgFe_2O_4$ samples at heating rates of 15, 20, 25, and 30 °C min^{-1}. From the Kissinger plot of the DSC data (Fig. 5(c)), it can be perceived that the activation energy, E_A, for the $MgFe_2O_4$-doped MgH_2 composite is 99.9 kJ mol^{-1}, which is decrease 33.1 kJ mol^{-1} compared with the milled MgH_2 (133.0 kJ mol^{-1}). The result indicates that addition of $MgFe_2O_4$ reduces the decomposition activation energy and boost the desorption performances of MgH_2.

Fig. 6 presents the microstructures of the pure and milled MgH_2, and $MgFe_2O_4$-doped MgH_2. From the images, it can be seen clearly that the particle size of the pure MgH_2 is around 50–100 μm (Fig. 6(a)). Fig. 6(b) shows the image of the MgH_2 after 1 h ball milling. The size of the milled MgH_2 was decreased dramatically compared to the pure MgH_2. However, the image shows agglomeration and inconsistent particle sizes. Fig. 6(c) shows that the particle size of 10 wt% $MgFe_2O_4$-doped MgH_2 was the smallest and had less agglomeration than the pure and milled MgH_2. Smallest particle size gives a larger region of contact to the MgH_2, thus resulting in the higher rate of reaction of MgH_2.

To investigate the phase structure, XRD measurement was performed on the 10 wt% $MgFe_2O_4$-doped MgH_2 sample, as shown in Fig. 7. From Fig. 7(a), it can be observed that the MgH_2 and $MgFe_2O_4$ phases are present in the as-milled $MgFe_2O_4$-doped MgH_2 sample. No additional peaks were found from the spectra. After dehydrogenation at 450 °C (Fig. 7(b)), the XRD pattern showed that the MgH_2 was completely dehydrogenated to Mg. This result demonstrates that the decomposition of MgH_2 was completed after heating for up to 450 °C. Furthermore, a small peak of MgO and Fe formed after the desorption process, thus demonstrate that the partial reaction of MgH_2 with $MgFe_2O_4$ may occur during the heating process as follows:

$$4MgH_2 + MgFe_2O_4 \rightarrow Mg + 4MgO + 2Fe + 4H_2 \tag{3}$$
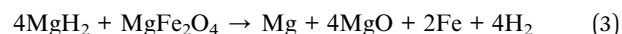
The standard Gibbs Free energy, ΔG_f°, of MgH_2, $MgFe_2O_4$ and MgO are −35.9824, −1317.1232 and −569.024 kJ mol^{-1},
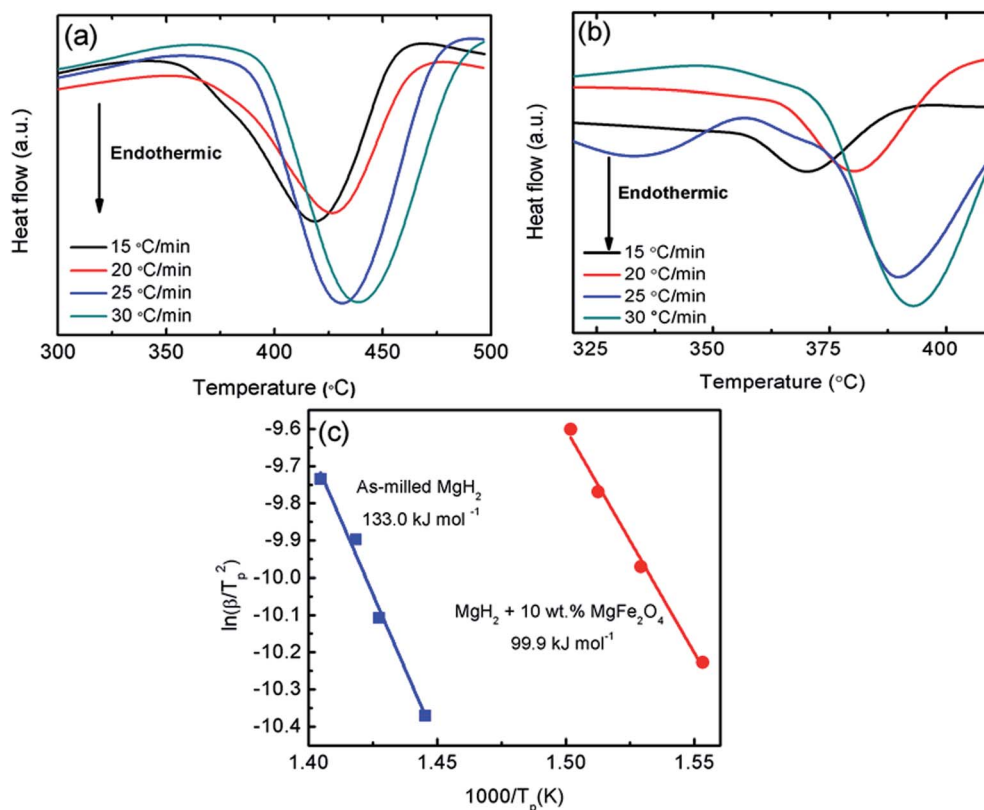
Fig. 5 DSC curves at heating rates of 15, 20, 25, and 30 °C min^{-1} for (a) milled MgH_2, (b) MgH_2 +10 wt% $MgFe_2O_4$ and (c) the Kissinger plot of decomposition for 10 wt% $MgFe_2O_4$-doped MgH_2 composite and milled MgH_2.
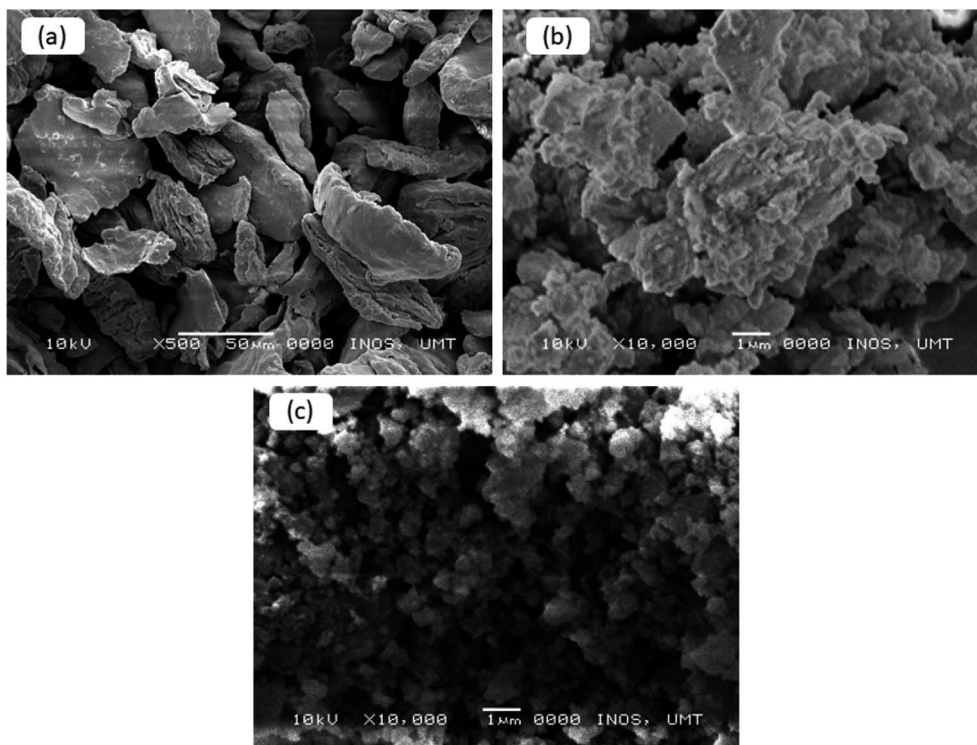
Fig. 6 SEM images for the pure MgH_2 (a), milled MgH_2 (b) and MgH_2 + 10 wt% $MgFe_2O_4$ (c).

respectively.[42] The total change ΔG correlated with the reaction in eqn (3) is -815.0168 kJ mol^{-1}. These values can confirm the possibility of the reaction in eqn (3) from thermodynamic potentials. Fig. 7(c) shows the XRD patterns for the rehydrogenated sample under 33.0 atm H_2 at 320 °C. The result illustrates that the phase of Mg was fully converted into MgH_2. Furthermore, the peak of Fe and MgO still remained after undergo rehydrogenation.

From the above analyses, the improvements in the sorption properties of MgH_2 doped with 10 wt% $MgFe_2O_4$ may be resulted from the formations of Fe and MgO. Fe and MgO may act as the real catalysts that play a vital role in the improvements of MgH_2 sorptions. Therefore, to verify the effect of Fe and MgO on MgH_2, samples of 10 wt% MgO-doped MgH_2 and 10 wt% Fe-doped MgH_2 were prepared and the TPD profiles for the dehydrogenations were shown as in Fig. 8. It is clearly seen that the decomposition temperature of MgH_2 are reduced with the addition of MgO or Fe as compared to the pure and milled MgH_2. However, the performance of these MgO and Fe are not significant as the sample of 10 wt% of $MgFe_2O_4$ doped with MgH_2. This demonstrated that the *in situ* generated MgO and Fe from the reaction of MgH_2 + 10 wt% of $MgFe_2O_4$ may play a significant role that introduce a synergetic catalytic effect that cause a significant improvement on the dehydrogenation performances of MgH_2 doped with 10 wt% of $MgFe_2O_4$. In addition, the *in situ* formed Fe and MgO in the MgH_2 + 10 wt% of $MgFe_2O_4$ sample are speculated to have a higher degree of dispersion and more compact phase segregation as compared to the milled MgH_2 + 10 wt% Fe and milled MgH_2 + 10 wt%

MgO. This would be likely to lead the improvement of the sorption kinetics.

From the result obtained, we postulate that formation of fresh and fine MgO and Fe species which resulted from the reaction between MgH_2 and $MgFe_2O_4$ during the dehydrogenation process may play significant role in improving the sorption performances of MgH_2. Numerous studies have claimed that the newly active species formed during the de/absorption process may play as a real catalyst in the enhancement of MgH_2 sorption.[43,44] Many works have proven that Fe is
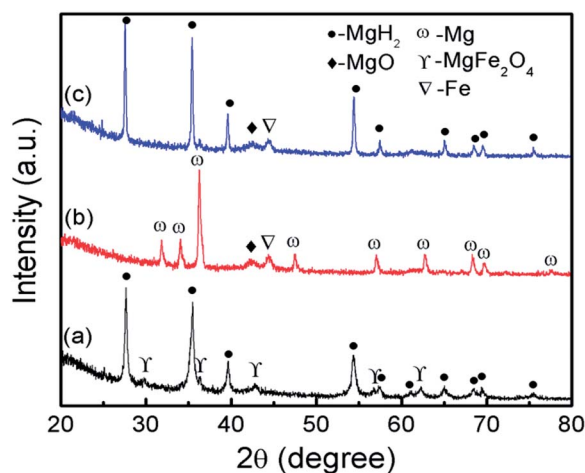

Fig. 7 XRD spectra of the MgH_2 + 10 wt% $MgFe_2O_4$ (a) after ball milling for 1 h, (b) after desorption under 1.0 atm at 450 °C and (c) after absorption under 33.0 atm at 320 °C.
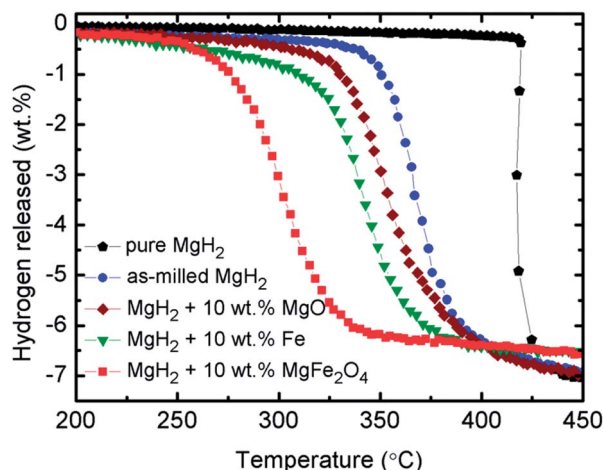
Fig. 8 Decomposition temperature profile of pure and milled MgH_2, 10 wt% MgO-doped MgH_2, 10 wt% Fe-doped MgH_2 and 10 wt% $MgFe_2O_4$-doped MgH_2 sample.

an excellent catalyst for sorption performance in MgH_2.[7-9] It is believed that the presence of fresh and fine Fe could interact with H_2 molecules, thus possibly leading to the dissociation of H_2 molecules and the improvement of the de/rehydrogenation kinetic. Furthermore, previous studies have shown that the sorption performance in MgH_2 can be enhanced with the addition of MgO. Ares-Fernández and Aguey-Zinsou[45] claimed that the addition of MgO to MgH_2 during the milling process led to an enhancement of sorption kinetics because of the high electronegativity MgO. In another study, the same group also claimed that during the milling process, MgO may act as a process control agent that can lead to the reduction of the particle agglomeration of MgH_2 by an optimal breakage rate, thus aiding the high stability of these particles and evading the use of cold welding.[46] Shan et al.[15] also revealed that MgO has a great catalytic effect on the MgH_2 sorption performance. Their study showed that during the heating process in $CoFe_2O_4$-doped MgH_2 composite system, MgO is formed. The catalytic effect of MgO could work together with the catalytic role of the Fe metal to create a synergetic effect. Therefore, the in situ active species of Fe and MgO may actually act as real catalysts and further enhance the hydrogen sorption performance of MgH_2. However, further studies are needed to elucidate more details on the exact role of $MgFe_2O_4$ addition in MgH_2.

4. Conclusion

In this study, nanolayer-like-shaped $MgFe_2O_4$ was successfully synthesised through a rapid, simple hydrothermal method. The addition of 10 wt% as-synthesised $MgFe_2O_4$ to MgH_2 reduces the onset decomposition temperature and enhances sorption kinetics. The $MgFe_2O_4$-doped MgH_2 sample has started to release H_2 at approximately 250 °C, 90 °C and 170 °C lower than milled and pure MgH_2 respectively. In a duration of 10 min, the isothermal desorption kinetic study showed that the doped sample can release

approximately 4.8 wt% H_2 at 320 °C while the milled MgH_2 only desorbed less than 1.0 wt% H_2 under the same condition. For isothermal absorption kinetics, the doped sample can absorb approximately 5.5 wt% H_2 in 10 min at 200 °C. By contrast, the milled MgH_2 sample absorbed only 4.0 wt% H_2 in the same condition. From the Kissinger analysis, the apparent activation energies, E_A, for the $MgFe_2O_4$-doped MgH_2 sample were calculated to be 99.9 kJ mol^{-1}, which is decreased by 33.1 kJ mol^{-1} compared with the milled MgH_2 (133.0 kJ mol^{-1}). The XRD exploration displays the formation of new species of Fe and MgO after the dehydrogenation process, and these species remained unchanged after rehydrogenation. It is believed that the new species of Fe and MgO play a synergistic role in enhancing the hydrogen storage performances of MgH_2.

Conflicts of interest

There are no conflicts to declare.

Acknowledgements

References

1 I. P. Jain, C. Lal and A. Jain, *Int. J. Hydrogen Energy*, 2010, **35**, 5133–5144.
2 L. Ouyang, J. Tang, Y. Zhao, H. Wang, X. Yao, J. Liu, J. Zou and M. Zhu, *Sci. Rep.*, 2015, **5**, 10776.
3 M. Polanski, J. Bystrzycki and T. Plocinski, *Int. J. Hydrogen Energy*, 2008, **33**, 1859–1867.
4 J. Huot, G. Liang, S. Boily, A. Van Neste and R. Schulz, *J. Alloys Compd.*, 1999, **293–295**, 495–500.
5 N. N. Sulaiman and M. Ismail, *Dalton Trans.*, 2016, **45**, 19380–19388.
6 M. A. Lillo-Ródenas, Z. X. Guo, K. F. Aguey-Zinsou, D. Cazorla-Amorós and A. Linares-Solano, *Carbon*, 2008, **46**, 126–137.
7 N. Hanada, T. Ichikawa and H. Fujii, *J. Phys. Chem. B*, 2005, **109**, 7188–7194.
8 H. Chen, H. Yu, Q. Zhang, B. Liu, P. Liu, X. Zhou, Z. Han and S. Zhou, *J. Power Sources*, 2016, **322**, 179–186.
9 G. Liang, J. Huot, S. Boily, A. Van Neste and R. Schulz, *J. Alloys Compd.*, 1999, **292**, 247–252.
10 S. A. Shevlin and Z. X. Guo, *J. Phys. Chem. C*, 2013, **117**, 10883–10891.
11 J. Lu, Y. J. Choi, Z. Z. Fang, H. Y. Sohn and E. Ronnebro, *J. Am. Chem. Soc.*, 2009, **131**, 15843–15852.
12 N. Patelli, M. Calizzi, A. Migliori, V. Morandi and L. Pasquini, *J. Phys. Chem. C*, 2017, **121**, 11166–11177.
13 N. S. Mustafa and M. Ismail, *J. Alloys Compd.*, 2017, **695**, 2532–2538.

14 D. Pukazhselvan, N. Nasani, P. Correia, E. Carbó-Argibay, G. Otero-Irurueta, D. G. Stroppa and D. P. Fagg, *J. Power Sources*, 2017, **362**, 174–183.

15 J. Shan, P. Li, Q. Wan, F. Zhai, J. Zhang, Z. Li, Z. Liu, A. A. Volinsky and X. Qu, *J. Power Sources*, 2014, **268**, 778–786.

16 Z. Jalil, A. Rahwanto, F. Mulana and M. Mustanir, *Int. J. Technol.*, 2016, **7**, 1301–1306.

17 T. Ma, S. Isobe, Y. Wang, N. Hashimoto and S. Ohnuki, *J. Phys. Chem. C*, 2013, **117**, 10302–10307.

18 M. S. Yahya and M. Ismail, *Int. J. Hydrogen Energy*, 2018, **43**, 6244–6255.

19 N. N. Sulaiman, N. S. Mustafa and M. Ismail, *Dalton Trans.*, 2016, **45**, 7085–7093.

20 L. P. Ma, X. D. Kang, H. B. Dai, Y. Liang, Z. Z. Fang, P. J. Wang, P. Wang and H. M. Cheng, *Acta Mater.*, 2009, **57**, 2250–2258.

21 N. N. Sulaiman, N. Juahir, N. S. Mustafa, F. A. Halim Yap and M. Ismail, *J. Energy Chem.*, 2016, **25**, 832–839.

22 D. Wu, L. Ouyang, C. Wu, H. Wang, J. Liu, L. Sun and M. Zhu, *J. Alloys Compd.*, 2015, **642**, 180–184.

23 X. B. Yu, Y. H. Guo, H. Yang, Z. Wu, D. M. Grant and G. S. Walker, *J. Phys. Chem. C*, 2009, **113**, 5324–5328.

24 X. B. Yu, Z. X. Yang, H. K. Liu, D. M. Grant and G. S. Walker, *Int. J. Hydrogen Energy*, 2010, **35**, 6338–6344.

25 J. Zhang, J. Shan, P. Li, F. Zhai, Q. Wan, Z. Liu and X. Qu, *J. Alloys Compd.*, 2015, **643**, 174–180.

26 P. Li, Q. Wan, Z. Li, F. Zhai, Y. Li, L. Cui, X. Qu and A. A. Volinsky, *J. Power Sources*, 2013, **239**, 201–206.

27 N. H. Idris, N. S. Mustafa and M. Ismail, *Int. J. Hydrogen Energy*, 2017, **42**, 21114–21120.

28 N. Juahir, N. S. Mustafa, A. Sinin and M. Ismail, *RSC Adv.*, 2015, **5**, 60983–60989.

29 Q. Wan, P. Li, J. Shan, F. Zhai, Z. Li and X. Qu, *J. Phys. Chem. C*, 2015, **119**, 2925–2934.

30 T. Zhang, S. Isobe, A. Jain, Y. Wang, S. Yamaguchi, H. Miyaoka, T. Ichikawa, Y. Kojima and N. Hashimoto, *J. Alloys Compd.*, 2017, **711**, 400–405.

31 T. Zhang, S. Isobe, Y. Wang, H. Oka, N. Hashimoto and S. Ohnuki, *J. Mater. Chem. A*, 2014, **2**, 4361–4365.

32 G. Xu, N. Shen, L. Chen, Y. Chen and W. Zhang, *Mater. Res. Bull.*, 2017, **89**, 197–203.

33 N. S. Mustafa, N. N. Sulaiman and M. Ismail, *RSC Adv.*, 2016, **6**, 110004–110010.

34 M. Baricco, M. W. Rahman, S. Livraghi, A. Castellero, S. Enzo and E. Giamello, *J. Alloys Compd.*, 2012, **536**(supplement 1), S216–S221.

35 M. S. Yahya and M. Ismail, *J. Energy Chem.*, 2018, DOI: org/10.1016/j.jechem.2017.10.020.

36 A. Pradeep, P. Priyadharsini and G. Chandrasekaran, *J. Magn. Magn. Mater.*, 2008, **320**, 2774–2779.

37 K. B. Modi, M. C. Chhantbar and H. H. Joshi, *Ceram. Int.*, 2006, **32**, 111–114.

38 Y. Yin, W. Liu, N. Huo and S. Yang, *ACS Sustainable Chem. Eng.*, 2017, **5**, 563–570.

39 Z. Yan, J. Gao, Y. Li, M. Zhang and M. Guo, *RSC Adv.*, 2015, **5**, 92778–92787.

40 Y. Liu, C. Liang, H. Zhou, M. Gao, H. Pan and Q. Wang, *Chem. Commun.*, 2011, **47**, 1740–1742.

41 H. E. Kissinger, *Anal. Chem.*, 1957, **29**, 1702–1706.

42 http://www.chemistry-reference.com/StandardThermodynamicValues.pdf.

43 Y. Cheng, W. Zhang, J. Liu, K. Cheng and Z. Zhao, *Int. J. Hydrogen Energy*, 2017, **42**, 356–365.

44 M. Ismail, N. S. Mustafa, N. Juahir and F. A. H. Yap, *Mater. Chem. Phys.*, 2016, **170**, 77–82.

45 J.-R. Ares-Fernández and K.-F. Aguey-Zinsou, *Catalysts*, 2012, **2**, 330.

46 K. F. Aguey-Zinsou, J. R. Ares Fernandez, T. Klassen and R. Bormann, *Mater. Res. Bull.*, 2006, **41**, 1118–1126.